Proceedings of the ASME 2019
International Mechanical Engineering Congress and Exposition
IMECE2019
November 11-14, 2019, Salt Lake City, UT, USA

IMECE2019-10672

FINITE ELEMENT ANALYSIS OF THE EFFECT OF POROSITY ON THE PLASTICITY AND DAMAGE BEHAVIOR OF MG AZ31 AND AL 6061 T651 ALLOYS

Allen Perkins
Mississippi State University
Mississippi State, MS, USA

Wenhua Yang
Mississippi State University
Mississippi State, MS, USA

Yucheng Liu
Mississippi State University
Mississippi State, MS, USA

Lei Chen
Mississippi State University
Mississippi State, MS, USA

Caleb Yenusah
Mississippi State University
Mississippi State, MS, USA

ABSTRACT

Porosity has been known to have a profound effect on a material's mechanical properties, often weakening the material. Highly porous metallic materials prove troublesome for supporting a load-based structure due to the voids that are present throughout the microstructure of the material. In this study, the previously developed ISV damage plasticity model is used to investigate the effect of the porosity on aluminum alloy 6061-T651 and magnesium alloy AZ31 through finite element analysis (FEA). It is determined that porosity has a profound impact on the strength of the aluminum alloy and much lesser effect on the magnesium alloy. Porosity is also shown to affect other properties of the materials, such as the hardness and pore growth.

INTRODUCTION

Porosity has long been studied as to its effects on the mechanical properties and microstructure of metallic materials. Porosity is represented by voids that exist throughout the material and are known to impact its mechanical properties. The voids are commonly created from several different factors such as general aging or as a result of some processing techniques. Magnesium and aluminum alloys are of interest in many industry applications due to their high strength and low-density properties. Magnesium is known to be lighter than aluminum and provide a more desirable strength-to-weight ratio. However, aluminum is more widely used due to its better hardness and better resistance to wear[1].

Voids are prone to be formed in aluminum alloys during common manufacturing processes such as heat treatment [2]. Aluminum alloys are of interest to industry similar to magnesium because of its high strength-to-weight ratio. This feature enables its use in many applications where lightweight designs are preferred. These alloys are also known to be resistive to corrosion, making them ideal for humid and corrosive environments [3].

As previously mentioned, magnesium alloys have also drawn great interest due to their high strength along with its low density. This has made it an optimal option in structural applications, especially those dealing with automotive or aerospace. Despite these advantages, there are several concerns that limit the application of magnesium and a strong interest has arisen in improving these properties. Some of the concerns are that magnesium's strength is known to suffer at high temperatures and is also known to offer poor corrosion resistance when compared to other metals. Corrosion severely limits the implementation of magnesium in several types of environments in which corrosion is expected to occur rapidly. Corrosion in magnesium alloys has been reported to correlate with the porosity present in their microstructures. As the porosity increases, so does the corrosion of the material [4]. Several methods have been presented to improve the corrosion resistance such as refining the grain size [5] or by increasing the aluminum content in the material [6]. Furthermore, several processing techniques have been examined including caliber rolling [7] and diecasting [8, 9] to improve magnesium's mechanical properties in various applications. However, some

of these techniques have been found to affect the porosity of the material by altering its microstructure.

THEORETICAL BACKGROUND

Internal state variable (ISV) theory has been developed and expanded upon over the course of the past 20-30 years through numerous contributions. It is most commonly used to study inelastic behavior of materials and can potentially be used to study almost any type of material. It is intended to be employed for the purpose of predicating mechanical properties based on the mechanical history of a material [10]. Bamman and Horstemeyer made several contributions to this theory to develop the ISV model for predicting plasticity and damage of metallic materials. Horstemeyer et al. continued to expand the damage model to include a representation of factors such as void nucleation, growth, and coalescence [11]. In their model, a damage variable, ϕ, is introduced to capture the damage behavior of materials, which is the ratio of the change in volume between the elastically unloaded state to the volume in the initial reference state (V_v) with respect to the volume in the elastically unloaded state (V_2) (Eqn. 1) [11].

$$\phi = \frac{V_v}{V_2} \tag{1}$$

The Void nucleation, $\eta(t)$, was defined in Eqn. (2), in which a, b, c are material parameters, C_{coeff} is a constant value for the material, $\varepsilon(t)$ denotes the strain, I, J_2, and J_3 are stress invariants, f is the volume fraction of the second phase material, and d is the average silicon particle size.

$$\eta(t) = C_{coeff} \exp\left(\frac{\varepsilon(t) d^{1/2}}{K_{IC} f^{1/3}} \left\{ a\left[\frac{4}{27} - \frac{J_3^2}{J_2^3}\right] + b\frac{J_3}{J_2^{3/2}} + c\left\| \frac{I_1}{\sqrt{J_2}} \right\| \right\}\right), \tag{2}$$

The void growth, υ_v is indicated in Eqn. (3), where R_0 is the initial void radius and n is a constant based on the material. This equation follows the McClintock void growth rule.

$$\upsilon_v = \frac{4}{3}\left(R_0 \exp\left[\varepsilon(t)\frac{\sqrt{3}}{2(1-n)} \times \sinh\left(\sqrt{3}(1-n)\frac{\sqrt{2}I_1}{3\sqrt{J_2}}\right)\right]\right)^3 \tag{3}$$

A representation of the coalescence of the voids during the damage evolution process was accounted for by Eqn (4). As shown in that equation, the coalescence is related to the volume fraction of the second phase, f.

$$C = 1 + f(\eta, \upsilon_v) \tag{4}$$

These damage parameters were then factored into the calculations of the material parameters of the model to complete the plasticity-damage model. In this model, the material is assumed to fail as ϕ approaches 1. The ISV's representation of the voids existing in the microstructure with respect to the damage and plasticity of a material was expected to provide extensive information that would depict a correlation between the properties of a material and its porosity. For this reason, the ISV model developed by Horstemeyer was ideal for the purpose of this study. In fact, this model had been applied to study microstructural effects on failure and damage of metallic materials [12-16].

This model integrates various material constants that have been determined from experimental results for the plasticity and damage behavior of the materials [17]. These calibrated values can be used to define a material's properties such that the mechanical behavior of the material may be demonstrated through the FEA results yielded from this model. The plasticity of a material is largely represented by the various material C constants, which are used to model a material's behavior in terms of yield stress, kinematic hardening, and isotropic hardening. Porosity within a material's microstructure is known to cause material failure and damage. This parameter is one of the criteria considered by the ISV model in determining the material behavior. Thereby the influence of porosity on a material's plasticity and damage behavior can be determined through this ISV model. Porosity is implemented into the ISV code in terms of the void volume fraction. It should be noted that in this study, the terms void volume fraction and the porosity of a material are synonymous. By altering this value for the material damage parameters, the effect of porosity may be determined by implementing the ISV model through the finite element method. In this study, some assumptions were applied when using this model. First, the shape of the void was assumed as spherical shape and it would not change during the FEA simulations. Also, it had been noted by other researchers that the shape of the voids have a rather minimal effect on the failure of a material [18]. Similarly, the void size was assumed to remain constant throughout the simulation. This was also expected to have a minimal impact in the results since the change of the void size was very small during the simulations. Finally, the voids were assumed to be distributed throughout the material homogeneously due to a limitation in the current state of the ISV model. The current model does not consider the pore distribution, and this associates a homogeneity with respect to the voids present throughout the material.

This study will evaluate the effect of porosity on the plastic, failure, and damage behaviors of Magnesium AZ31 and Aluminum 6061-T651 alloys employing the present ISV model.

FINITE ELEMENT ANALYSIS

The impact of porosity was determined during this study though the implementation of the previously developed internal state variable model. This model will predict material weakening and failure through experimentally determined

material constants. A tensile loading scenario is a commonly employed method to determine material strength and durability and was deemed ideal for this study. This is to be accomplished using the guidance of the ASTM E8 standard, which defines the methodology for an experimental tension test. The specimen model was created according to this standard and implemented into the FEA, whose constitutive property was defined using the ISV model. Different levels of porosity were assigned to the model through altering the initial void volume fraction of the ISV model. The specimen models with different porosity levels were then used for FEA simulations to reveal the effect of the porosity on the material's mechanical behavior.

The selected materials were designed to be tested through a state of tensile loading; therefore, the model was designed according to the ASTM standard E8 [19]. This standard defines the test specimen that should be used throughout a tension test, for three different widths. For this study, the 40mm width was used, which is the widest specimen as stated by the standard, as shown in Fig. 1. The corresponding dimensions shown Fig.1 are listed in Table 1.

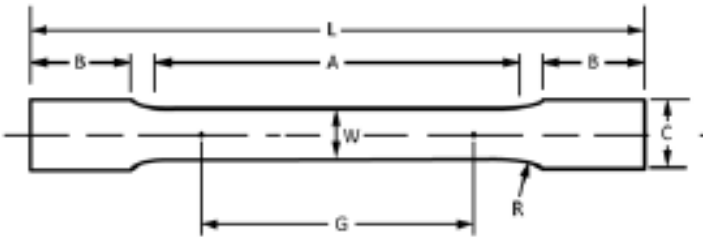

FIGURE 1: DEFINED DIMENSIONS BY ASTM E8 FOR A TENSION TEST SPECIMEN.

TABLE 1: TEST SPECIMEN DIMENSIONS USED TO DESIGN THE TENSION TEST SPECIMEN.

Gauge Length (G)	200mm
Width (W)	40mm
Thickness (T)	5mm
Radius of Fillet (R)	25mm
Overall Length (L)	450mm
Length of Reduced Parallel Section (A)	225mm
Length of Grip Section (B)	75mm
Width of Grip Section (C)	50mm

The FEA simulations were conducted using Abaqus Explicit (Simulia). A mesh using an eight-node linear brick element with reduced integration (denoted as C3D8R in the Abaqus element library) was deemed to be an appropriate element. The ISV model used was verified through a comparison of experimental and FEA results in [11], and further verification of the model was not performed in this study. Because of this reason, the reduced integration was employed to minimize the computational cost of the analysis. An approximate global seed size of 5.6 was assigned to construct the mesh featuring 1971 nodes and 1152 elements. The part was partitioned until a structured meshing technique could be successfully performed to define an accurate mesh. The mesh was verified by considering its average aspect ratio of 1.18. The worst aspect ratio of the mesh was a value of 1.27, which was still well within the commonly accepted range. Additional relax stiffness and element deletion controls were ascribed to the mesh for the purposes of this simulation.

For this analysis, a strain rate method was used throughout the finite element simulation. A displacement loading condition was applied to the model at a rate of 0.05mm/s as commonly undergone by tension tests following the E8 standard. This was accomplished by defining a constant displacement boundary condition to the top cell of the tensile bar. Since damage of the material is significant to the purpose of this study, the model was strained until failure was attained. This was visually represented by implementing element deletion through the material input file. The simulation was completed upon the failure of the specimen models and the stress-strain curves were extracted for further discussions.

The boundary conditions were modeled to faithfully represent the constraints applied on the specimens during experimental tension tests. The bottom cell of the FEA model was fully fixed in all directions using an ENCASTRE boundary condition. The top cell was then fixed in all but the y-direction through the implementation of a displacement boundary condition. The loading and boundary conditions are illustrated in Fig. 2. These conditions were applied to the simulation through a dynamic, explicit step. Due to the non-linear nature of elastic-plastic relations, non-linearities were considered in the solver.

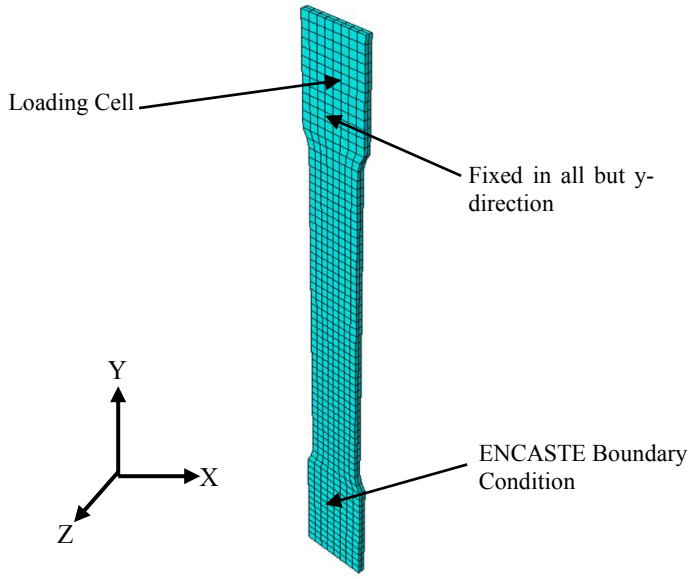

FIGURE 2: FINITE ELEMENT MODEL MESH AND LOADING AND BOUNDARY CONDITIONS.

The ISV model requires DMG plasticity and damage parameters that have been previously determined. The material properties and constants for the ISV damage model are shown for the magnesium AZ31 and aluminum 6061-T651 alloys in Table 2 and Table 3 respectively.

TABLE 2: MATERIAL PROPERTIES AND ISV CONSTANTS OF MAGNESIUM AZ31

Material Properties		**DMG Damage**	
Density (ρ)	1780 (kg/m^3)	a	1000
Young's modulus (E)	45 (GPa)	b	1000
Poisson's ratio	0.35	c	1000
DMG Plasticity		C_{coeff}	2000
C_1	4.3	Fracture toughness (K_{IC})	50
C_2	296	D	0.01
C_3	3.37	*f*	0.001
C_4	1060	C_{d1}	1
C_5	0.00001	C_{d2}	1
C_7	0.7463	Reference grain size (DCS_0)	30
C_8	1.173	Grain size of the material (DCS)	30
C_9	39186	nn	0.002
C_{10}	78.8	Initial void radius (R_0)	0.001
C_{11}	0.00594		
C_{12}	1.21×10^{-7}		
C_{13}	0.21075		
C_{14}	3.315×10^{-7}		
C_{15}	9085.5		
C_{16}	17.8		

The void volume fraction (porosity, denoted as V_{vfi} in the ISV model) is an important DMG damage parameter and has a significant effect on the FEA results. As previously mentioned, various values were entered for this parameter to demonstrate the effect of porosity on the mechanical behavior of the specimens. A profound literature review was performed to decide the appropriate range for porosity levels for the aluminum and magnesium alloys, from which realistic porosity levels could be selected for the simulations. Wang, et. al conducted a study on the failure analysis of AZ31 magnesium alloy sheets [20]. This study modified the Gurson-Tvergaard-Needleman (GTN) model to yield a VUMAT sub routine file to evaluate the damage evolution of the material. In this study, porosity was treated as a state variable and was analyzed through the finite element method. The resulting porosity of

TABLE 3: MATERIAL PROPERTIES AND ISV CONSTANTS OF ALUMINUM 6061-T651

Material Properties		**DMG Damage**	
Density (ρ)	2700 (kg/m^3)	b	180000
Young's modulus (E)	68.9 (GPa)	c	500
Poisson's ratio	0.33	C_{eff}	0.0001
DMG Plasticity		Fracture toughness (K_{IC})	1000
C_1	6	d	0.0048
C_3	276	*f*	1
C_5	1	C_{d1}	0.0069
C_9	2007.67	C_{d2}	0.002
C_{13}	0.451353	Reference grain size (DCS_0)	20
C_{15}	657.53	Grain size of material (DCS)	20
		nn	0.3
		Initial void radius (R_0)	0.0001

their model consisted within the approximate range of zero to 9% (0.09). A separate study conducted by Wang, et. al to evaluate porous material used varying void volume fractions from 0.01 to 0.12 [21]. Therefore, void volume fractions of 0.0001, 0.02, 0.04, 0.06, and 0.08 were chosen for this study to represent typical porosity levels in the analyzed alloys. The first value of 0.0001 served as a baseline for the results in which the porosity is largely negligible. A similar study that also used the GTN model, produced similar results as well for the void volume fraction [22]. The same range was applied to all materials considered in this study for the purpose of comparison.

In the FEA simulation, the test specimen was pulled in tension at a constant strain rate to a point until fracture was achieved. Fracture was considered to occur when the damage variable $\phi = 1$. This was visually demonstrated through the simulation by the specimen breaking at this point. To compile the results of the simulation, the output data was averaged over the elements of the gauge length of the tensile bar. These values would yield an indication as to the behavior of the material during the simulation. The numerical results for the damage of the material was the only variable not evaluated in gauge region. It was evaluated for at the region of fracture, where it reached 1 to indicate failure.

RESULTS

Magnesium AZ31 Alloy:

By implementing the ISV model, the behavior of the magnesium AZ31 alloy could be defined to characterize the

influence of different levels of porosity in its microstructure. The stress-strain relationships of the models with the selected porosity levels are plotted in Fig. 3. The displayed curves suggest an inverse relationship between the porosity and the strength of the material. This relationship indicates that the voids will weaken the material as more are present in the microstructure. It can also be seen that the point of material failure is not affected by the porosity. This is further exemplified through the damage evolution throughout the simulation.

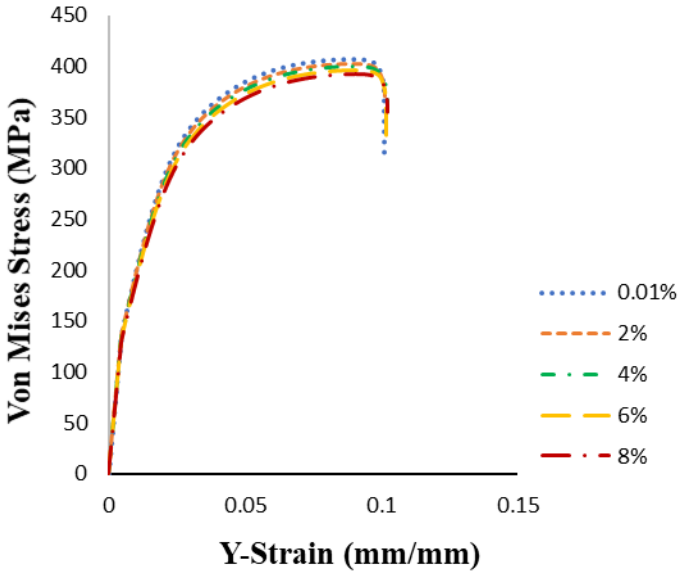

FIGURE 3: VON MISES STRESS VERSUS TOTAL STRAIN IN Y-DIRECTION.

Fig. 4 shows the relationship between the damage and the plastic equivalent strain for various porosity values. The damage of the material increased initially along with the values of porosity, but material failure occurred at the same strain for each specimen. This phenomenon indicates that the porosity does not affect the failure of the magnesium alloy, which is in congruence with the findings presented in Fig. 3. One point of interest indicated by Fig. 3 is that the damage remains at a relatively low value until the specimen fractures. This corresponds closely to the behavior of magnesium as reported in [23].

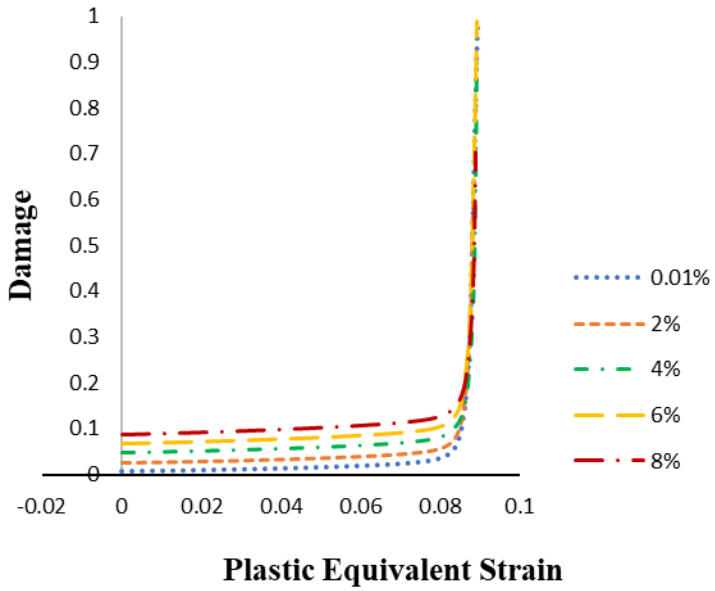

FIGURE 4: DAMAGE GRAPHED WITH RESPECT TO THE PLASTIC EQUIVALENT STRAIN.

Fig. 5 displays a contour plot of the damage at a state before fracture occurs and the Von Mises stress at the state immediately following fracture of the specimen. It can be seen from that figure that the damage value in red regions is close to 1. Those regions indicate the fracture locations predicted in the simulation.

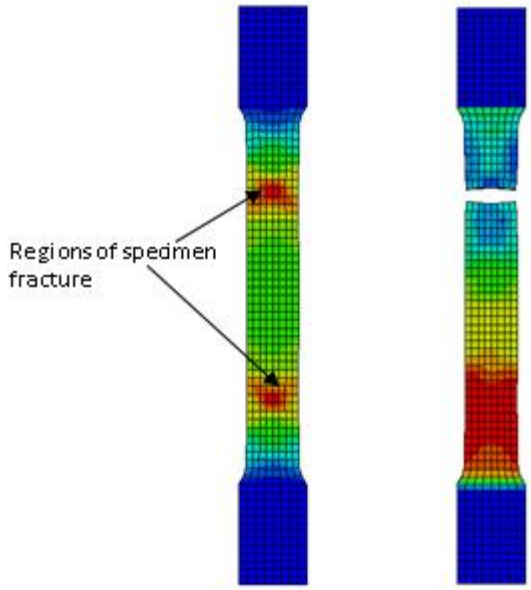

FIGURE 5: CONTOUR PLOT OF DAMAGE (LEFT) AND VON MISES STRESS (RIGHT) AT STATE OF MATERIAL FRACTURE.

Aside from the strength, porosity is known to influence the material hardness. The relationship between the porosity and the hardness is best demonstrated through the isotropic and kinematic hardening values, as shown in Figs. 6 and 7. These

figures show that the porosity does affect the hardness of the material, but not in a significant manner.

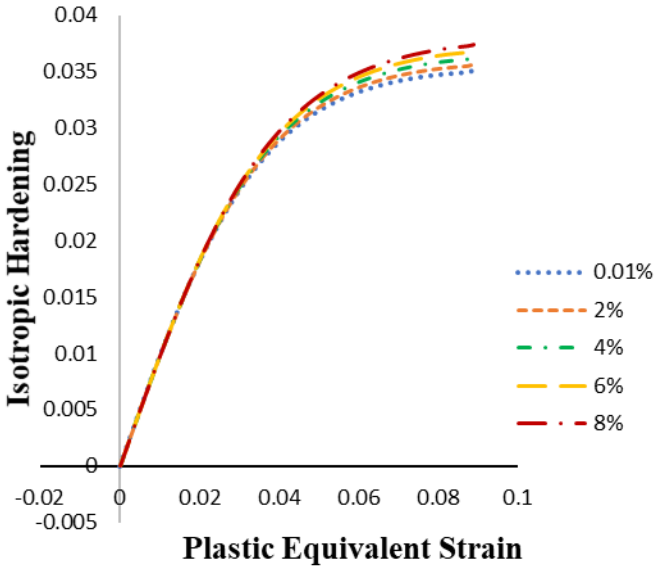

FIGURE 6: RELATIONSHIP BETWEEN ISOTROPIC HARDENING AND PLASTIC EQUIVALENT STRAIN.

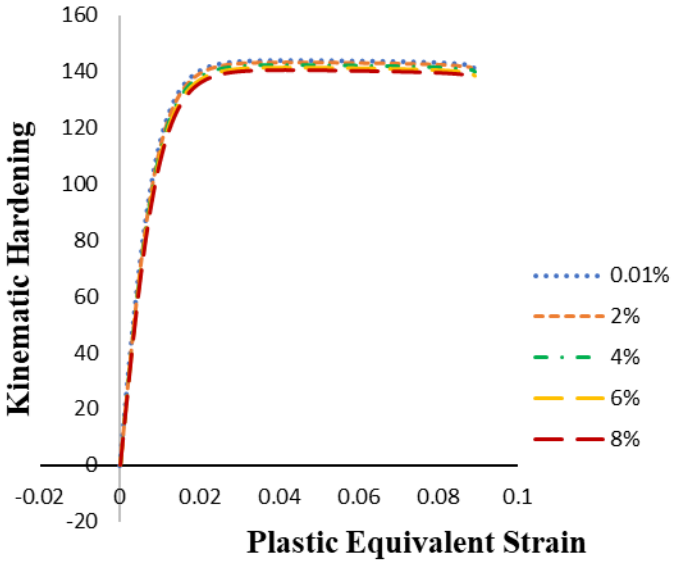

FIGURE 7: RELATIONSHIP BETWEEN KINEMATIC AND PLASTIC EQUIVALENT STRAIN.

Higher levels of porosity will also affect the rate at which more voids are nucleated and developed within the material microstructure. This is demonstrated through the results in Fig. 8. This plot accounts for the original voids present in the microstructure and show how they grow as the strain is applied. It can be seen from the slope of each of the lines, that higher porosity levels will increase the nucleation rate of new pores and growth rate of existing pores.

In summary, the porosity will affect the properties of the magnesium alloy but not at a level of profound significance.

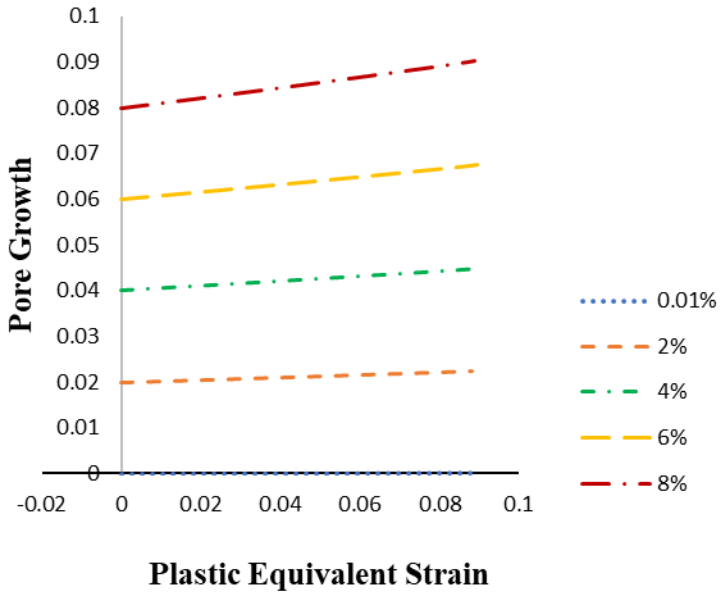

FIGURE 8: RATE OF PORE GROWTH WITH RESPECT TO THE PLASTIC EQUIVALENT STRAIN.

Aluminum 6061-T651:

Influence of porosity on the properties of Aluminum 6061-T651 alloy was also investigated using the ISV model. The aluminum alloy displayed an increase in the elongation of the elements until fracture occurred and the highest damage was much more concentrated in the center of the specimen when compared to the results of the magnesium alloy. The damage and von mises stress before and after the fracture of the specimen through the simulation are shown by Fig. 9.

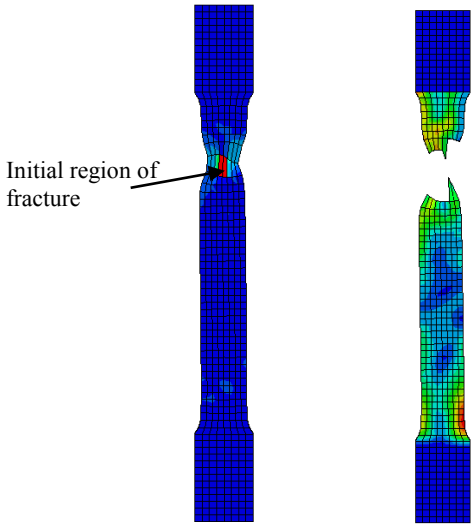

FIGURE 9: ALUMINUM 6061-T651 DAMAGE BEFORE FRACTURE (LEFT) AND VON MISES STRESS POST FRACTURE (RIGHT).

Fig. 9 highlights the increased ductility of the aluminum alloy when compared with the magnesium alloy as shown in the additional elongation of the aluminum alloy model. This is also indicated by the stress-strain relationships yielded from FEA simulations, as displayed in Fig. 10. It can be seen through this figure that porosity has a profound impact in the mechanical properties of the material. When the porosity is negligible, it can endure much higher straining than when porosity is introduced into the material. As the porosity levels increased, failure continued to occur at lower strain levels; however, the interval between the strains at which the failure occurred became less as the porosity increased. It can therefore be concluded that porosity causes a decrease in the ultimate tensile strength of the aluminum alloy, which agrees well with the results presented in [24].

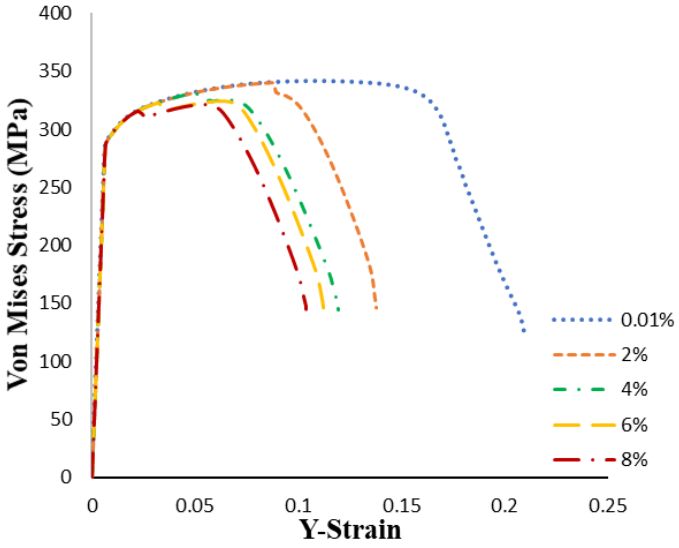

FIGURE 10: VON MISES STRESS-STRAIN CURVE FOR AL 6061-T651 ALLOY.

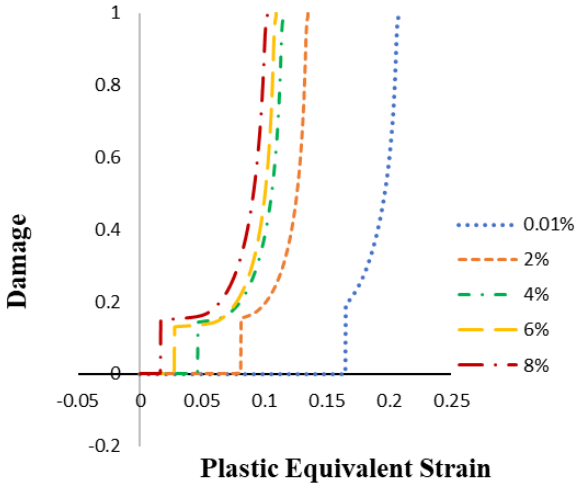

FIGURE 11: DAMAGE PLOTTED WITH RESPECT TO THE PLASTIC EQUIVALENT STRAIN FOR AL 6061-T651 ALLOY.

A similar relationship can be found from the damage evolution curves plotted in Fig. 11. As the porosity level increased, the strain level at which the damage approached failure decreased very fast. Furthermore, there is a large difference the damage evolution curve when the porosity is negligible and the curves at considerable porosity levels.

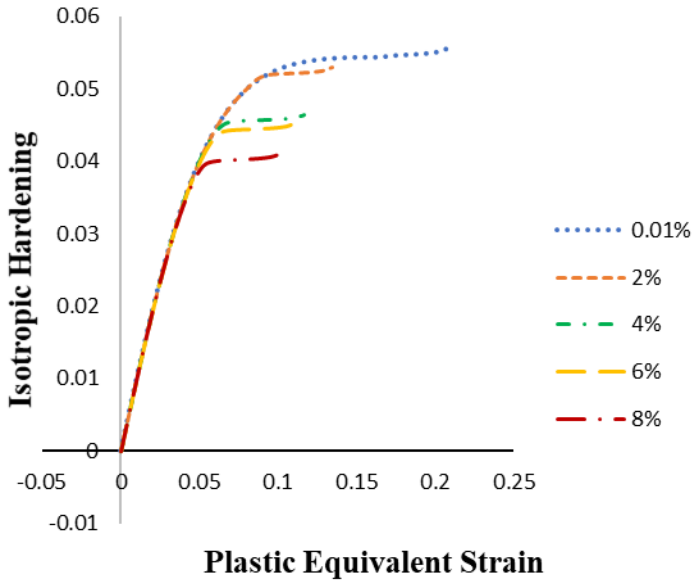

FIGURE 12: ISOTROPIC HARDENING WITH RESPECT TO THE PLASTIC EQUIVALENT STRAIN.

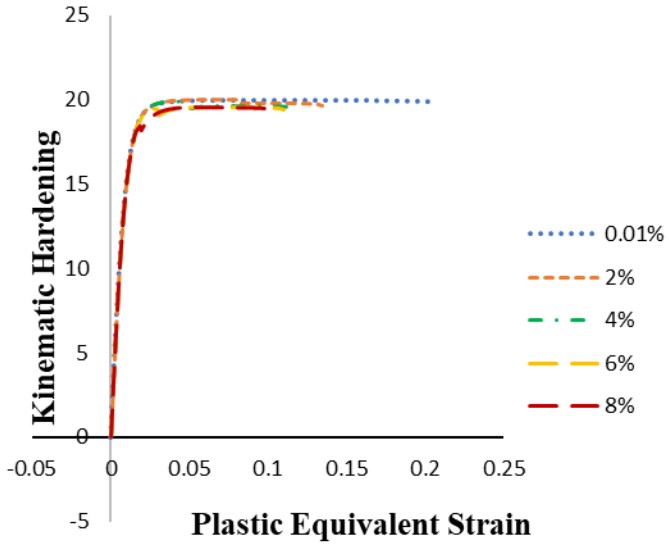

FIGURE 13: KINEMATIC HARDENING WITH RESPECT TO THE PLASTIC EQUIVALENT STRAIN.

Figs. 12 and 13 indicate the change in the hardness of the material through the relationships between the isotropic and kinematic hardening and the plastic equivalent strain. From those figures it can be seen that the kinematic hardening is not

affected by the porosity, but the isotropic hardening curves (Fig. 12) suggest that the material will soften as more porosity is present in its microstructure. The softening of the material is observed as the material approaches its point of failure at lower strain levels as the porosity increases. In Fig. 14, the relationships between the void growth rate and the strain for the aluminum alloy specimen with different porosity levels are plotted. From that figure it can be seen that the porosity dramatically affects the pores growth rate in the material. As the porosity increased, the voids began to grow at lower strains and the magnitude increased significantly.

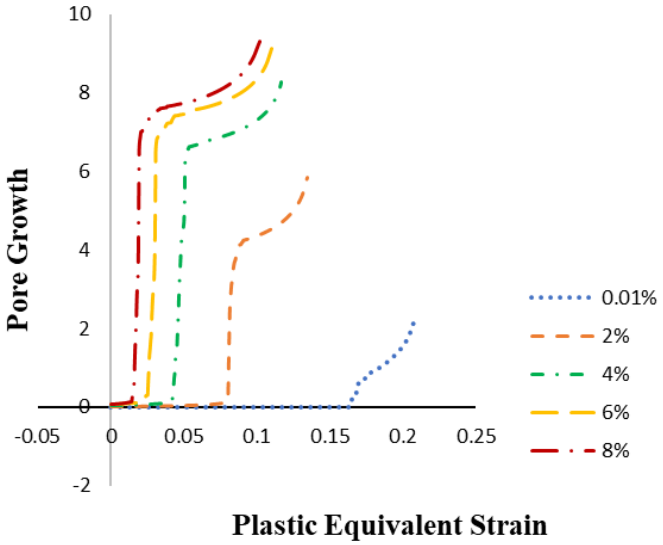

FIGURE 14: RELATIONSHIPS BETWEEN PORES GROWTH AND THE PLASTIC EQUIVALENT STRAIN.

Figs. 9 to 14 show that the porosity has unequivocal effects on the mechanical properties of aluminum 6061-T651.

DISCUSSION

The simulation results showed that porosity has a strong effect on the behavior of aluminum alloy 6061-T651 but is not as impactful for the magnesium alloy AZ31. Porosity has also been determined to be impactful for these metals in other loading situations as well. Other researchers have performed experimental analysis to find out the effect of porosity on these materials. For both magnesium and aluminum alloys, it was determined that in cases of fatigue, fracture almost exclusively initiates at voids in the microstructure [25], [26]. This is to be expected, but it further highlights the impact of the porosity within the material. Outcomes of this study also present an aspect of continued study by implementing the ISV damage model to consider cases of fatigue as well as considering the location of the porosity throughout the microstructure as to the effect on the material's damage evolution. The assumptions made for this study indicated the effect of porosity as a function of the number of voids in the material. Other areas of interest when considering a material's porosity would be to investigate the dispersion of the voids throughout the microstructure of a material and remove the homogeneity assumption. This also promotes future topics that the ISV model could be expanded to include. In addition, the shape and change in radius of the voids under different loading conditions are considerations that future studies could investigate.

CONCLUSION

In this study, the ISV damage model developed by Horstemeyer and Bamman was used to study the effect of porosity on aluminum 6061-T651 and magnesium AZ31 alloys. The porosity was shown to impact both of alloys, but the aluminum alloy was affected at a much higher rate. Material failure occurred in the aluminum alloy at a lower straining as the porosity increased, but no apparent effect was indicated for the failure of the magnesium alloy. This was confirmed through the material failure, which was indicated by the damage approaching a value of one. For both materials, the rate of pore growth was increased for higher porosity levels.

ACKNOWLEDGMENTS

This work is financially supported by NSF CMMI 1662854 and its REU supplement. The computer simulations were carried out on the clusters of High Performance Computing Collaboratory (HPC^2) at Mississippi State University. The authors recognize the Center for Advanced Vehicular Systems (CAVS) at Mississippi State University.

REFERENCES

[1] D. S. Mehta, S. H. Masood, and W. Q. Song, "Investigation of wear properties of magnesium and aluminum alloys for automotive applications," *J. Mater. Process. Technol.*, vol. 155–156, pp. 1526–1531, Nov. 2004.

[2] K. Hinode, I. Asano, and Y. Homma, "Void formation mechanism in VLSI aluminum metallization," *IEEE Trans. Electron Devices*, vol. 36, no. 6, pp. 1050–1055, Jun. 1989.

[3] H. Agarwal, A. M. Gokhale, S. Graham, and M. F. Horstemeyer, "Void growth in 6061-aluminum alloy under triaxial stress state," *Mater. Sci. Eng. A*, vol. 341, no. 1–2, pp. 35–42, Jan. 2003.

[4] G.L. Song and A. Atrens, "Corrosion Mechanisms of Magnesium Alloys," *Adv. Eng. Mater.*, vol. 1, no. 1, pp. 11–13, 2000.

[5] N. N. Aung and W. Zhou, "Effect of grain size and twins on corrosion behaviour of AZ31B magnesium alloy," *Corros. Sci.*, vol. 52, no. 2, pp. 589–594, Feb. 2010.

[6] M. Liu *et al.*, "Calculated phase diagrams and the corrosion of die-cast Mg–Al alloys," *Corros. Sci.*, vol. 51, no. 3, pp. 602–619, Mar. 2009.

[7] A. Tripathi, S. V. S. N. Murty, and P. R. Narayanan, "Microstructure and texture evolution in AZ31 magnesium alloy during caliber rolling at different temperatures," *J. Magnes. Alloys*, vol. 5, no. 3, pp. 340–347, Sep. 2017.

[8] C. H. Cáceres, W. J. Poole, A. L. Bowles, and C. J. Davidson, "Section thickness, macrohardness and yield strength

in high-pressure diecast magnesium alloy AZ91," *Mater. Sci. Eng. A*, vol. 402, no. 1–2, pp. 269–277, Aug. 2005.
[9] C. H. Cáceres, J. R. Griffiths, A. R. Pakdel, and C. J. Davidson, "Microhardness mapping and the hardness-yield strength relationship in high-pressure diecast magnesium alloy AZ91," *Mater. Sci. Eng. A*, vol. 402, no. 1–2, pp. 258–268, Aug. 2005.
[10] M. F. Horstemeyer and D. J. Bammann, "Historical review of internal state variable theory for inelasticity," *Int. J. Plast.*, vol. 26, no. 9, pp. 1310–1334, Sep. 2010.
[11] M. F. Horstemeyer, J. Lathrop, A. M. Gokhale, and M. Dighe, "Modeling stress state dependent damage evolution in a cast Al–Si–Mg aluminum alloy," *Theor. Appl. Fract. Mech.*, vol. 33, no. 1, pp. 31–47, Feb. 2000.
[12] G. He, Y.-Q. Dou, X. Guo, and Y.-C. Liu, "Computational investigation of effects of grain size on ballistic performance of copper", *International Journal for Computational Methods in Engineering Science & Mechanics*, 19(1), 2018, 1-10.
[13] Y.-Q. Dou, Y.-C. Liu, Y. Hammi, and W. Whittington, "Application of a microstructure-based ISV plasticity damage model to study penetration mechanics of metals and validation through penetration study of aluminum", *Modelling and Simulation in engineering*, 6189168, 2017, 1-10.
[14] G. He, Y.-C. Liu, Y.-Q. Dou, and X. Guo, "Effects of grain size on ballistic response of copper materials", IMECE2017-70585, Proceedings of ASME 2017 International Mechanical Engineering Congress & Exposition, Tampa, FL, USA, November 3-9, 2017.
[15] Y.-Q. Dou, Y.-C. Liu, and Y. Hammi, "Computational investigation of high velocity penetration of copper subjected to impact from nickel projectiles", IMECE2015-50241, Proceedings of ASME 2015 International Mechanical Engineering Congress & Exposition, Houston, TX, USA, November 13-19, 2015.
[16] Y.-Q. Dou, Y.-C. Liu, and Y. Hammi, "Comparison of Johnson-Cook model and an ISV plasticity damage model in penetration simulation", IMECE2016-68195, Proceedings of ASME 2016 International Mechanical Engineering Congress & Exposition, Phoenix, AZ, USA, November 11-17, 2016.
[17] Y.-Q. Dou, Y.-C. Liu, W. Whittington, and J. Miller, "Experimental calibration of ISV damage model constants for pure copper for high-speed impacts simulation", IMECE2016-65690, Proceedings of ASME 2016 International Mechanical Engineering Congress & Exposition, Phoenix, AZ, USA, November 11-17, 2016.
[18] Y. X. Gao, J. Z. Yi, P. D. Lee, and T. C. Lindley, "The effect of porosity on the fatigue life of cast aluminium-silicon alloys*," *Fatigue Fract. Eng. Mater. Struct.*, vol. 27, no. 7, pp. 559–570, 2004.
[19] E28 Committee, "Test Methods for Tension Testing of Metallic Materials," ASTM International.
[20] R. Wang, Z. Chen, Y. Li, and C. Dong, "Failure analysis of AZ31 magnesium alloy sheets based on the extended GTN damage model," *Int. J. Miner. Metall. Mater.*, vol. 20, no. 12, pp. 1198–1207, Dec. 2013.
[21] D.-A. Wang, J. Pan, and S.-D. Liu, "An Anisotropic Gurson Yield Criterion for Porous Ductile Sheet Metals with Planar Anisotropy," *Int. J. Damage Mech.*, vol. 13, no. 1, pp. 7–33, Jan. 2004.
[22] P. J. Zhao, Z. H. Chen, and C. F. Dong, "Damage and Failure Analysis of AZ31 Alloy Sheet in Warm Stamping Processes," *J. Mater. Eng. Perform.*, vol. 25, no. 7, pp. 2702–2710, Jul. 2016.
[23] A. K. Ray and D. S. Wilkinson, "The effect of microstructure on damage and fracture in AZ31B and ZEK100 magnesium alloys," *Mater. Sci. Eng. A*, vol. 658, pp. 33–41, Mar. 2016.
[24] Z. Ma, "Effect of Iron-Intermetallics and Porosity on Tensile and Impact Properties of Aluminum-Silicon-Copper and Aluminum-Silicon-Magnesium Cast Alloys." Order No. NQ76012, Universite du Quebec a Chicoutimi (Canada), Ann Arbor, 2002.
[25] H. Mayer, M. Papakyriacou, B. Zettl, and S. E. Stanzl-Tschegg, "Influence of porosity on the fatigue limit of die cast magnesium and aluminium alloys," *Int. J. Fatigue*, vol. 25, no. 3, pp. 245–256, Mar. 2003.
[26] H. Ammar, A. Samuel, and F. Samuel, "Porosity and the fatigue behavior of hypoeutectic and hypereutectic aluminum–silicon casting alloys," *Int. J. Fatigue*, vol. 30, no. 6, pp. 1024–1035, Jun. 2008.